The Effect of Discharge Chamber Wall Temperature on Ion Thruster Performance

Paul J. Wilbur* and John R. Brophy†
Colorado State University, Fort Collins, Colorado

Experiments conducted on a ring cusp ion thruster that could be maintained at temperatures in the range 90-500 K during operation by cooling it with liquid nitrogen are described. The measured changes in performance induced by discharge chamber wall temperature changes are compared to those predicted by a simple discharge chamber model. Good agreement between the temperature-induced effects predicted by the model and measured results are demonstrated. Decreases in wall temperature to ~90 K are shown to effect substantial improvements in performance.

Introduction

FOR many years it has been assumed that neutral atoms in an ion thruster discharge chamber move at a velocity determined by the mean discharge chamber wall temperature.[1-3] By applying this assumption, it has been possible to make useful predictions of neutral atom density levels and charge exchange ion production rates in ion thrusters. This assumption also makes it possible to predict that the performance of a discharge chamber can be improved by lowering the mean discharge chamber wall temperature. The extent of the performance improvement that could be induced by such a wall temperature reduction has, however, not been demonstrated. Further, the validity of the presumed relationship between discharge chamber wall temperature and neutral atom velocity has not been verified experimentally.

The intent of the work described herein is to demonstrate the extent of performance improvements induced by reductions in wall temperature and to show that a recently proposed discharge chamber model[4] describes the magnitude of these improvements correctly. Various perturbing effects that might cause the atom temperature to differ from the mean wall temperature are also examined theoretically.

Theory

The direct measurement of the velocity distribution function or the mean velocity of neutral atoms in an ion thruster discharge chamber is difficult to accomplish; however, indirect measurements based on discharge chamber performance can be used to infer the neutral atom velocities. In the present case, it is assumed that the neutral atoms are in thermal equilibrium with discharge chamber walls and that the relationship between the neutral atom mean velocity and measured discharge performance variables is described by the simple discharge chamber model proposed in a companion article.[4] It is argued that agreement between measured changes in performance induced by wall temperature changes and those predicted by the model suggest both the model and the neutral atom/wall thermal equilibration assumption are correct.

While the model in its complete form in intended to predict complete discharge chamber performance curves, only a portion of the model will be needed here. This portion relates the energy cost of a plasma ion (ϵ_P) to the discharge chamber neutral density parameter $\dot{m}(1-\eta_u)$ through

$$\epsilon_P = \epsilon_P^* \left[1 - e^{-C_0 \dot{m}(1-\eta_u)}\right]^{-1} \tag{1}$$

where $\dot{m}$ is the propellant flow rate and η_u is the propellant utilization efficiency. The primary electron utilization factor C_0 in this equation is defined[4] to be

$$C_0 \equiv 4\sigma_0 \ell_e / e v_0 A_g \phi_0 \tag{2}$$

where σ_0 is the total inelastic collision cross section for primary electron-neutral atom collisions, ℓ_e the primary electron containment length, e the electron charge, A_g the grid area, ϕ_0 the grid transparency to neutral atoms, and v_0 the velocity of the neutral atoms. None of these parameters should depend on the discharge chamber wall temperature except the neutral atom velocity. This velocity is the mean velocity for a Maxwell-Boltzmann distribution function and is given by

$$v_0 = \sqrt{8kT_0/\pi m} \tag{3}$$

where k is Boltzmann's constant and m is the mass of a propellant atom. The neutral atom temperature T_0 is determined by the state of collisional equilibrium achieved between these neutral atoms and the other particles or surfaces with which they interact—in this case, the ions, electrons, and discharge chamber wall surfaces exposed to the plasma. Because of the low atom and ion densities in an ion source discharge chamber (typically of order 10^{12} cm^{-3} and 10^{11} cm^{-3}, respectively), atoms will have frequent collisions with the walls. One would therefore have the first-order expectation of an atom temperature near the mean wall temperature ($T_0 = T_W$). Using this equality together with Eq. (2) yields

$$C_0 = (4\sigma_0 \ell_e / e A_g \phi_0)\sqrt{\pi m / 8kT_W} \tag{4}$$

The suitability of Eqs. (1) and (4) to describe correctly the relationship between the energy cost of a plasma ion (ϵ_P) and the neutral density parameter $\dot{m}(1-\eta_u)$ has been demonstrated experimentally in a companion article.[5]

Equation (4) indicates that the primary electron utilization factor C_0 should be a function of the discharge chamber wall

Received Aug. 1, 1984; revision submitted Feb. 11, 1985.

*Professor, Department of Mechanical Engineering. Member AIAA.

†Research Assistant, Department of Mechanical Engineering; presently at the Jet Propulsion Laboratory, Pasadena, CA. Member AIAA.

temperature. Consequently, the average plasma ion energy cost ϵ_P given by Eq. (6) should also be a function of the wall temperature. Further, it is postulated (and demonstrated experimentally later) that the baseline plasma ion energy cost ϵ_P^* is independent of the wall temperature. Thus, measured changes in the plasma ion energy cost resulting from a change in the discharge chamber wall temperature indicate a change in the value of the primary electron utilization factor. In this paper, changes in the primary electron utilization factor predicted by Eq. (4) are compared to the changes in this factor measured in an operating ion source in which the discharge chamber wall temperature is varied.

Apparatus and Procedure

In order to study experimentally the influence of discharge chamber wall temperature on discharge chamber performance, the ion source shown schematically in Fig. 1 was built. It is similar to the source described in Ref. 5, which was built to study the effects of discharge voltage, propellant, grid extraction area, and transparency on discharge chamber performance. The primary difference between these sources is the cooling coil installed for this experiment. This coil, which was made using 1.3 cm diam copper tubing compressed until it deformed plastically onto the steel shell, can be connected to a liquid nitrogen source. The liquid nitrogen flow rate through the coil is adjusted to control the steel shell temperature at values ranging from ~80 to ~500 K. The heat transfer area and contact thermal conductance are sufficiently high so that wall temperature measured using the iron-constantan thermocouples shown in Fig. 1 can be held within ~10 K of the liquid nitrogen boiling point (77 K) when the ion source is operated at maximum power.

The ion source of Fig. 1 has a 15 cm inside diameter steel shell, but the screen grid is masked down by the magnet support flange so that the ion beam diameter is only 12 cm. The magnetic field in the discharge chamber is produced by the upstream 1.9 cm×2.6 cm rectangular magnet, the central ring magnet assembly, and the downstream ring magnet assembly shown in Fig. 1. Each of the magnet assemblies shown has been made by placing 1.9 cm×1.3 cm×0.5 cm thick samarium cobalt magnets end to end and side to side to form the ring and rectangular magnet assemblies, respectively. The flux density at the surface of the magnet assemblies is 0.27 T, and the magnets are arranged so that the inner surface of the central ring magnet has a polarity opposite to those at the inner surfaces of the rectangular and downstream magnet assemblies. The central ring magnet assembly is insulated from the strip of 0.13 mm thick steel that serves as the discharge chamber anode shown in Fig. 1 by a piece of 0.076 mm thick flexible mica. Both the magnet assemblies and the anode are held in place by magnetic attraction forces between the magnets, the steel anode, and the steel shell.

In designing and building the discharge chamber, special attention was given to features that would minimize temperature differences between points on the discharge chamber wall and between the walls and the grid assembly. For example, the steel shell is 0.5 cm thick, and joints in the shell are silver-soldered together. The magnet support flange, which is made of 0.18 cm thick copper, is also soldered to the shell. A 0.7 mm thick steel ring is sandwiched in good mechanical contact between the copper flange and the magnet ring. The screen grid is clamped directly to the copper flange. The molybdenum screen grid is 0.43 mm thick and has a physical transparency of 68%. The molybdenum accelerator grid is 0.53 mm thick and has a physical transparency of 57%. The screen and accelerator grids were held at +1 and −0.5 kV, respectively, during the conduct of the tests.

A pair of 0.25 mm diam, 8 cm long tungsten wires, connected in parallel and heated to thermionic emission temperatures by passing an alternating current through them, serves as the cathode. The maximum cathode power applied at the highest electron emission condition required for these tests was ~200 W. The source was designed so that either argon or krypton propellant could be fed into it through the reverse flow feed line shown in Fig. 1. Flow rates of 500, 1000, and 1500 mA eq were used for both propellants. With argon the discharge voltage was maintained at 50 V, and with krypton 40 V was used. These voltages were selected as sufficient to yield stable discharge operation yet low enough to limit doubly charged ion production.

A special feature of the thruster was that the screen grid, downstream ring and rectangular magnet assemblies, steel shell, and magnet support flange were all connected in parallel to a power supply that could be used to bias these surfaces relative to cathode potential. By biasing these surfaces ~30 V negative of cathode potential, essentially all discharge chamber electrons could be repelled from these surfaces and, as a result, the ion current to them could be measured. By adding this current to the beam current, one obtains a value for the ion production rate J_P. The error between this measured ion production rate and the true one is equal to the ion losses to the anode that have not been in-

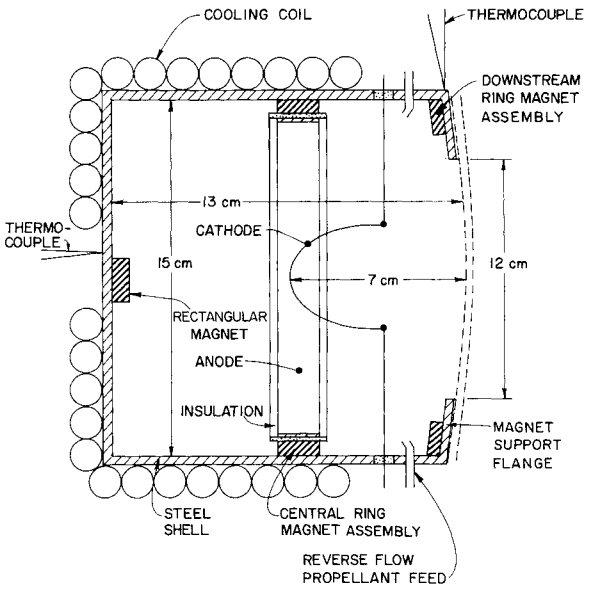

Fig. 1 Liquid nitrogen cooled ion source schematic.

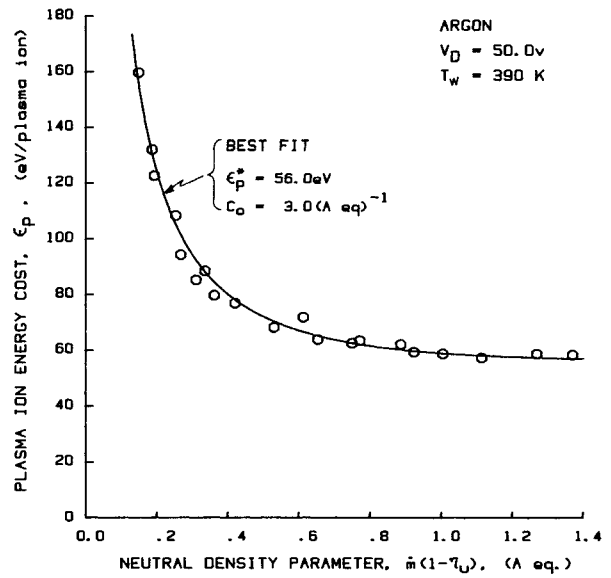

Fig. 2 Plasma ion performance correlation for argon at 390 K.

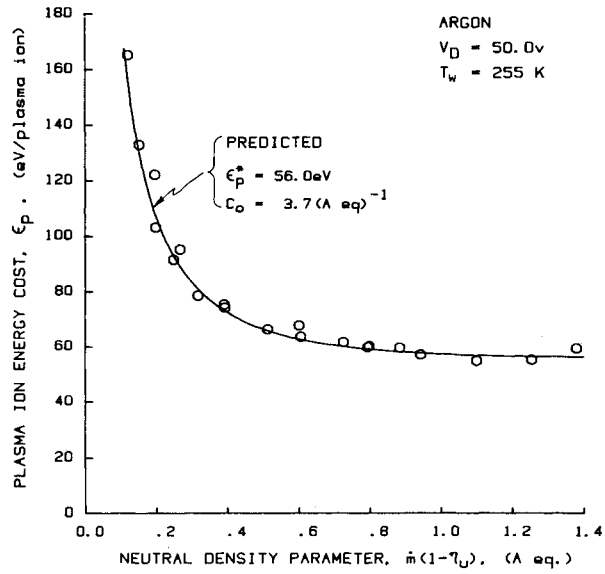

Fig. 3 Plasma ion performance correlation for argon at 255 K.

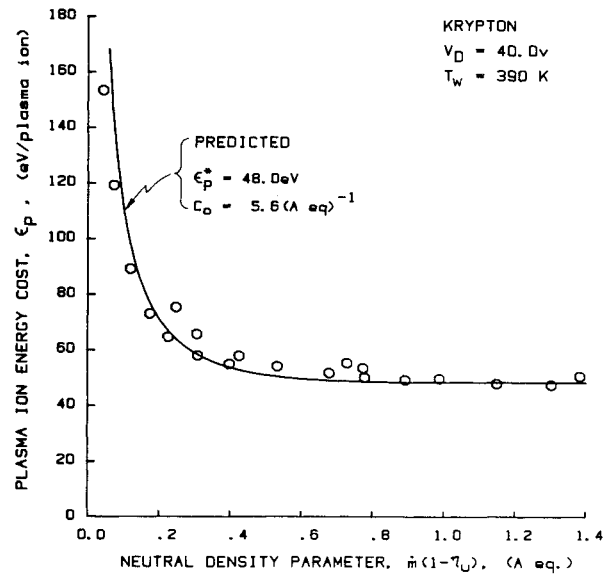

Fig. 5 Plasma ion performance correlation for krypton at 390 K.

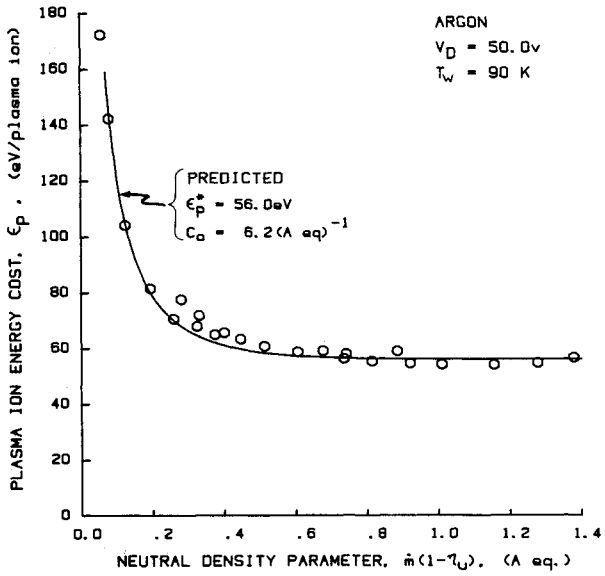

Fig. 4 Plasma ion performance correlation for argon at 90 K.

cluded in the measurement. This error has been estimated to be less than a few percent, based on the effective area for ion loss to the anode compared to other ion loss areas. Using the measured ion production rate J_P, the energy cost of a plasma ion ϵ_P can be computed using the following expression developed in the companion article[5]:

$$\epsilon_P = (J_D - J_P) V_D / J_P \tag{5}$$

In order to conduct the tests, the ion source was first allowed to stabilize thermally at a low discharge current level and a fixed propellant flow rate and discharge voltage. The discharge current was then increased in increments by increasing the cathode filament current while the flow rate and discharge voltage were held constant. At each discharge current the beam current and ion current to the steel shell and screen grid were recorded along with the discharge current. This procedure was repeated at three different flow rates at each wall temperature condition for argon and krypton propellants. The data were evaluated by computing the total ion production current as the sum of the beam current and ion current to the screen grid and shell. Equation (5) was then used to determine the average energy cost of a plasma ion. The neutral density parameter $[\dot{m}(1-\eta_u)]$, which is proportional to the neutral density, was also computed as the difference between the neutral propellant flow in A eq and the beam current. The fraction of the ions produced in the discharge chamber that are extracted into the beam f_B was also computed as the ratio of beam current J_B to total ion production current J_P.

Error Considerations

The temperature of propellant atoms in the discharge chamber is determined by collisions with wall surfaces and influenced by discharge plasma ions and electrons. There are two general sources of errors that could cause the atom temperature to differ from the measured mean wall temperature. They are: 1) variations in wall temperature that complicate the computation of the appropriate mean temperature from the measured values and 2) perturbations in the atomic temperature induced either by atomic collisions with electrons and ions or an influx of atoms having energies that differ markedly from those associated with the mean wall temperature. The magnitude of errors that might be expected from these two effects are now considered separately.

Wall Temperature Variation Effects

The worst-case wall temperature variations are realized when the discharge chamber and cathode are operated at maximum power. At this operating condition it is estimated that 200 W of power could be radiated from the cathode and the plasma. This power is assumed to be distributed uniformly over the interior surfaces of the chamber. Other power inputs to the walls are associated with electron and ion losses to these surfaces. Electrons are assumed conservatively to have an average energy of 10 eV and to flow to the anode at a rate given by the discharge current (4 A maximum). Ions, on the other hand, are assumed to go primarily into the beam, the grid webbing, and the grid support flange.

A consideration of the thermal conduction characteristics of the various component parts of the discharge chamber, along with the heat loads on these parts, suggests that the screen grid, anode, and cathode surfaces can be expected to perturb the mean wall temperature away from the values measured on the steel shell. The worst-case temperature profiles over each of the surfaces have therefore been determined, and the impact of these temperatures on the mean wall surface temperature has been evaluated. The screen grid

has the greatest effect because: 1) it has a low thermal conductivity as a result of its thin, perforated configuration, 2) it has a substantial area, and 3) it has a high distributed heat load as a result of direct ion impact over its surface.

In modeling the grids thermally, it was assumed that the extracted beam current was at its maximum value of 0.9 A. Since the extracted ion fraction for this source was typically 60% of the total ion production, this means that 0.6 A of ion current goes to interior surfaces of the discharge chamber. Assuming a screen grid transparency to ions of 80% gives an ion current of 0.22 A to the screen grid webbing and the remainder (0.38 A)to other surfaces accepting ions. It was also assumed that the ion current density to the screen grid webbing was the same as that through the screen grid holes and that ions striking the webbing had been accelerated from a worst-case plasma potential (~ 50 V) to screen grid bias potential (-30 V). This heat load, combined with the radiated one, induced a worst-case temperature at the screen grid centerline that was ~ 125 K above the temperature at the inner edge of the magnet support flange (Fig. 1). It was next assumed that all ions produced in the discharge chamber that did not go into the beam or onto the screen grid webbing (0.38 A) were directed uniformly onto the magnet support flange at an energy of 80 eV. Because this plate was made of copper and was thicker than the screen grid, the worst-case temperature difference computed between its inside edge (6 cm radius) and its outer one (7.5 cm radius) was only ~ 7 K.

The difference in temperature between the anode surface and the steel shell was computed by considering the heat flux to the interior surface of the anode resulting from both the electron current and radiated power from the cathode and plasma. It was assumed that the relatively soft mica was pressed firmly enough between the magnets and the anode itself so that contact thermal resistances were small and the major resistance to heat transfer occurred in the mica. Under these conditions the temperature difference between the anode and the steel shell was approximately 1 K. The cathode wire temperature was assumed to be the value required to assure thermionic emission (~ 1475 K).

When the area-weighted mean temperature of the surfaces exposed to the plasma was computed from the worst-case component temperatures just cited, it was found to be only ~ 7 K above the mean steel shell temperature. Hence, under worst-case thermal loading conditions, the mean wall temperature would be expected to be 7 K above the mean steel shell temperature. During the actual conduct of the test, the two thermocouples shown in Fig. 1 agreed to within about 5 K, and they were found to exhibit worst-case drifts of ~ 10 K during the conduct of a test in the temperature range 80 to 160 K, and ~ 5 K during the conduct of the higher-temperature tests. Based on these measurements and calculations, it is suggested that mean wall temperatures agree with measured ones to within ± 10 K for low-temperature tests and ± 5 K for higher temperature ones.

Collisional Effects

The neutral atom temperature could conceivably differ from the mean wall temperature because of collisions with electrons and ions that have energies substantially different from those associated with the unperturbed atom temperature. Electrons, because of their mass mismatch with the atoms, would not, however, be expected to perturb the atomic temperature significantly, even though their temperature is typically quite high (~ 10 eV $= 110{,}000$ K). Ions, on the other hand, could affect the atom temperature because they have a larger elastic, energy transfer cross section; they can undergo charge exchange reactions with atoms; and they can be accelerated to substantial energies by electric fields in the plasma. For typical discharge chamber configurations the ion energies can generally reach the electron temperature ($\lesssim 10$ eV), as determined by the Bohm criterion,[6] but will probably not exceed it. Typical elastic collision cross sections between argon or krypton ions and atoms lie below 10 Å^2 at the low ($\lesssim 10$ eV) energies involved.[7] For a typical ion density of 10^{11} cm^{-3}, this corresponds to a mean free path greater than 100 m, which is 700 times the discharge chamber dimensions. Hence, collisions with walls should dominate and elastic collision effects should be negligible. For the charge exchange process,[8,9] the argon and krypton cross sections are higher (of the order of 50 Å^2), but this still implies mean free paths of the order of 100 times the discharge chamber dimensions so that this collisional event would also be unlikely compared to wall collisions.

Finally, it is noted that ions that go to discharge chamber walls rather than being extracted into the beam are accelerated into the walls through plasma-to-wall potential difference of the order of several tens of volts. These ions, while they could recombine and come into thermal equilibrium with the wall before they leave it, might also be expected to recombine and recoil from it with some fraction of their incident energy. While it was hoped that the error due to recombined ions recoiling from the walls with energies above those expected for particles in thermal equilibrium with the walls would be small, no conclusive evidence was found in the literature to substantiate a supposition that this would or would not be the case.

Results

When the ion source was operated on argon at a wall temperature of 390 K and a discharge voltage of 50 V, the plasma ion energy cost and neutral density parameter data pairs indicated by the data symbols of Fig. 2 were computed from the measured data. Through trial and error selection of the parameters ϵ_P^* and C_0, Eq. (1) was fitted to these data. The fit, shown by the solid line in Fig. 2, was obtained for a primary electron utilization factor C_0 of 3.0 (A eq)$^{-1}$ and a baseline plasma ion energy cost ϵ_P^* of 56 eV. The baseline plasma ion energy cost is determined to first order by the propellant and the energy of the primary electrons (i.e., the discharge voltage), so that one would not expect it to be affected by changes in wall temperature. Changes in wall temperature should, however, cause the primary electron utilization factor to change in accordance with Eq. (4), and this equation could be applied directly if values for all of the quantities appearing in it were known. While most of the values are known, a validated model for the primary electron containment length ℓ_e has unfortunately not been developed at this point. One can still see if the model describes the physical situation adequately, however, by determining the value of the primary electron utilization factor appropriate to one wall temperature, then changing the wall temperature while holding all else constant and determining if the predicted change in C_0 is consistent with Eq. (4). This has been done here by taking the value of the primary electron utilization factor obtained by curve-fitting the data of Fig. 2 ($C_{0\,\mathrm{ref}}$) and computing new values of the factor appropriate to any new wall temperature from the following equation, which has been derived from Eq. (4):

$$C_0 = C_{0\,\mathrm{ref}} \sqrt{390/T_W} \tag{6}$$

Doing this, one predicts that the primary electron utilization factor should be 3.7 (A eq)$^{-1}$ for the case where argon propellant is used at a mean wall temperature of 255 K. Using this value of C_0, the solid line shown on Fig. 3 is predicted. When the ion source was operated at this wall temperature, the data points shown on Fig. 3 were measured. The agreement between these measured data points and the predicted curve is observed to be excellent. Applying Eq. (6) for a mean wall temperature of 90 K one obtains $C_0 = 6.2$ (A eq)$^{-1}$. This corresponds to the solid curve shown in Fig.

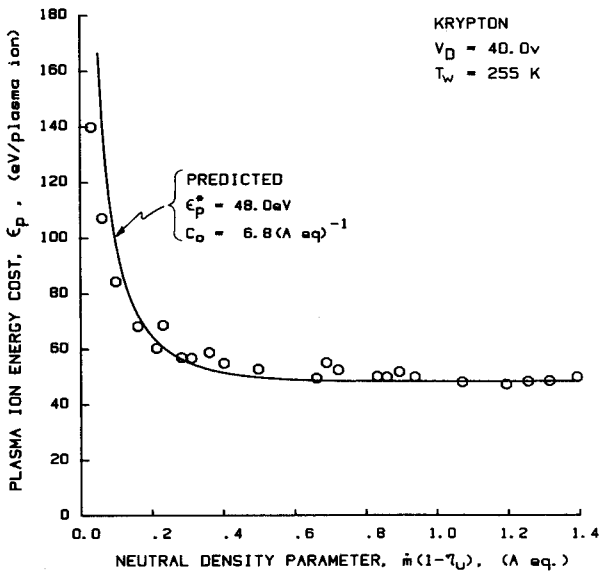

Fig. 6 Plasma ion performance correlation for krypton at 255 K.

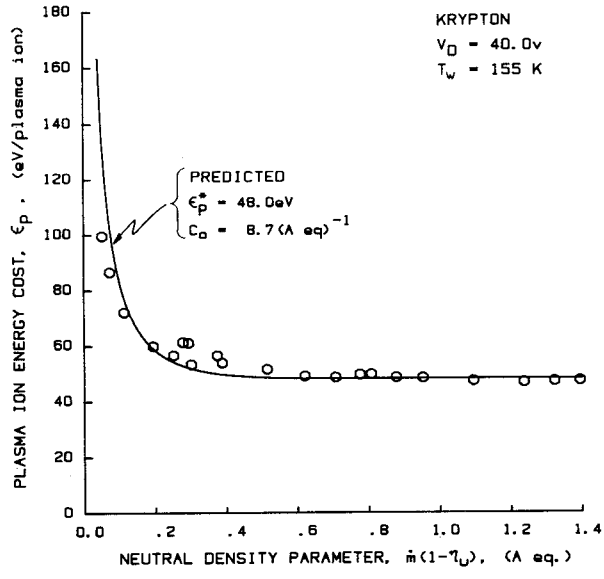

Fig. 7 Plasma ion performance correlation for krypton at 155 K.

4. When plasma ion energy cost/neutral density parameter data pairs were measured with the ion source operating at 90 K, the results shown by the data points on Fig. 4 were obtained. Again, the agreement between theory (solid line) and experiment (data points) appears to be good.

The ion source was also operated on krypton propellant at a mean wall temperature of 390 K. In order to predict the performance with this new propellant, the primary electron utilization factor was computed from the expression

$$C_0 = C_{0\,\mathrm{ref}} \frac{\sigma_{0_{\mathrm{Kr}}}}{\sigma_{0_{\mathrm{Ar}}}} \sqrt{\frac{m_{\mathrm{Kr}}}{m_{\mathrm{Ar}}}} \tag{7}$$

where the subscripts Kr and Ar pertain to krypton and argon, respectively. Using the appropriate atomic masses and total inelastic collision cross sections for argon at 50 V and krypton at 40 V as obtained from deHeer[10] in Eq. (7), one finds that $C_0 = 5.6$ (A eq)$^{-1}$ should be appropriate. The baseline energy cost per plasma ion ϵ_P^* would also be expected to change with the propellant and discharge voltage. Its value was selected in the present case for krypton from experimental data as the plasma ion energy cost at a high neutral density parameter, i.e., high flow rate/low beam current operating condition and was found to be 48 eV. Using $C_0 = 5.6$ A eq^{-1} and $\epsilon_P^* = 48$ eV in Eq. (1), the solid line shown in Fig. 5 was predicted for operation on krypton at 390 K. The discharge chamber performance data measured with krypton at 390 K are shown by the data symbols on Fig. 5. Once again, the agreement between the predicted and measured performance is good. For a krypton-fed discharge chamber cooled to 255 and 155 K, values of the primary electron utilization factor C_0 equal to 6.8 and 8.7 (A eq)$^{-1}$, respectively, are predicted by Eqs. (6) and (7). Using these values as input to Eq. (1), the solid lines of Figs. 6 and 7 are predicted. Measured data for these temperatures are again shown by the data symbols in these two figures. As in all previous cases, the measured data agree well with the predicted curves. It is noted that discharge chamber wall temperatures could not be reduced to ~90 K when krypton propellant was being used because the propellant tended to condense.

The results shown in Figs. 3 through 7 all show sufficiently close agreement between predicted and measured performance results to suggest that the effect of wall temperature is properly modeled in Eqs. (1) and (4). Changes in the primary electron utilization factor C_0 of ±10% were

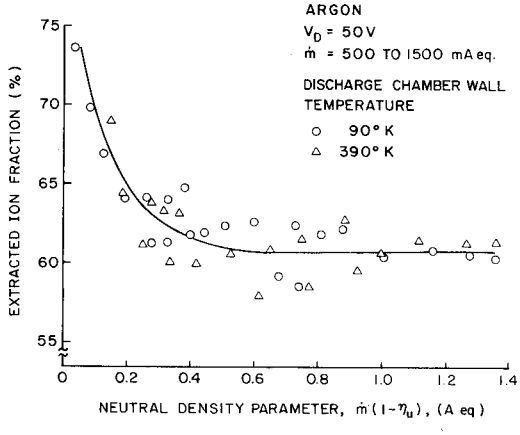

Fig. 8 Effect of discharge chamber wall temperature on extracted ion fraction.

generally sufficient to cause predicted curves in the figures to depart from the measured data to a degree that could be recognized readily. As a result, it is suggested that values of this factor are accurate to within about ±10% and that the wall temperature, which is proportional to the square of C_0, is therefore modeled by Eq. (4) to an accuracy within about ±20%.

The fraction of the ions produced in the discharge chamber that were extracted into the ion beam was also measured at each operating condition for these tests. Typical extracted ion fraction data are shown in Fig. 8 for argon propellant and discharge chamber wall temperatures of 90 K and 390 K. The data show the trend pointed out in Ref. 5, namely, that the extracted ion fraction is dependent on the neutral density parameter only at low values of this parameter. While there is some scatter in the data of Fig. 8, it is not actually very substantial, considering the expanded vertical scale used. More importantly, Fig. 8 shows no separation of the data caused by changes in wall temperature. This leads to the conclusion that the extracted ion fraction is independent of discharge chamber wall temperature as one would expect.

Conclusions

Substantial improvements in discharge chamber performance are induced by reductions in the mean discharge chamber wall temperature. The extent of these improvements

are predicted by the simple discharge chamber model described by Eqs. (1) and (4). Based on the high degree of agreement realized between the predictions of this model and experimental results, it is concluded that the assumptions of the model are valid. These assumptions are 1) that the atoms present in a typical ion thruster discharge move at a mean thermal velocity determined to first order by the mean discharge chamber wall temperature and 2) that this mean velocity is not perturbed significantly by collisional or recombined-ion recoil effects.

Acknowledgments

The development of the liquid nitrogen cooled ion source used in this work resulted from a discussion with Graeme Aston of the Jet Propulsion Laboratory. Dr. Aston suggested that such a source would be useful in conducting an experiment on the effect of neutral atom temperature on the divergence characteristics of ion beamlets. Once such a source had been made, its usefulness for the conduct of the experiments described in this paper was recognized. This contribution to the work by Dr. Aston is gratefully acknowledged. This work was supported by NASA Grant NGR-06-002-112.

References

[1]Masek, T. D., "Plasma Properties and Performance of Mercury Ion Thrusters," AIAA Paper 69-256, March 1969.

[2]Knauer, W., "Power Efficiency Limits of Kaufman Thruster Discharges," AIAA Paper 70-177, Jan. 1970.

[3]Kerslake, W. R., "Charge-Exchange Effects on the Accelerator Impingement of an Electron-Bombardment Ion Rocket," NASA TN-D1657, May 1963.

[4]Brophy, J. R. and Wilbur, P.J., "Simple Performance Model for Ring and Line Cusp Ion Thruster," *AIAA Journal*, Vol. 23, Nov. 1985, pp. 1731-1736.

[5]Brophy, J. R. and Wilbur, P.J., "An Experimental Study of Cusped Magnetic Field Discharge Chambers," *AIAA Journal*, Vol. 24, Jan. 1986, pp. 21-26.

[6]Bohm, D., "Minimum Ionic Kinetic Energy for a Stable Sheath," in *The Characteristics of Electrical Discharges in Magnetic Fields*, edited by A. Guthrie and R. K. Wakerling, McGraw-Hill Book Co., New York, 1949.

[7]Robinson, R. S., "Physical Processes in Directed Ion Beam Sputtering," NASA CR-159567, March 1979.

[8]Dillon, J. A. Jr., Sheradin, W. F., Edwards, H. D., and Ghosh, S. N., "Charge Transfer Reactions in Monatomic and Diatomic Gases," *Journal of Chemical Physics*, Vol. 23, 1955, pp. 776-779.

[9]Hasted, J. B., "The Exchange of Charge Between Ions and Atoms," *Proceedings of the Royal Society (London)* A205, Vol. 421, 1951.

[10]deHeer, F. J. et al., "Total Cross Sections for Electron Scattering by Ne, Ar, Kr and Xe," *Journal of Physics B: Atomic and Molecular Physics*, Vol. 12, No. 6, 1979, pp. 979-1002.